Chinese Chemical Letters 37 (2026) 111775

Contents lists available at ScienceDirect

Chinese Chemical Letters

journal homepage: www.elsevier.com/locate/cclet

High-temperature dielectric composite with excellent capacitive energy storage by multiscale chemical configuration design

Yuyan Du[a], Jinxia Cai[b], Tianyu Li[c,d,*], Yandong Hu[a], Haibo Zhang[e], Bing Xie[a,*]

[a] School of Power and Energy, Jiangxi Key Laboratory of Green General Aviation Power, Nanchang Hangkong University, Nanchang 330063, China
[b] Key Laboratory of Advanced Display and System Applications of Ministry of Education, Shanghai University, Shanghai 200072, China
[c] School of Materials Science and Engineering, University of Science and Technology Beijing, Beijing 100083, China
[d] Department of Physics, City University of Hong Kong, Hong Kong, China
[e] School of Materials Science and Engineering, Huazhong University of Science and Technology, Wuhan 430074, China

ARTICLE INFO

Article history:
Received 9 July 2025
Revised 16 August 2025
Accepted 29 August 2025
Available online 29 August 2025

Keywords:
Dielectric capacitors
High temperature
Inorganic-polymer composite
Free volume
Breakdown strength
Multiscale chemical design

ABSTRACT

Polymer dielectric capacitors are crucial for advanced power electronics but are often limited by the trade-off among energy density, efficiency, and thermal stability under high electric fields. To overcome these challenges, we propose a multiscale chemical configuration design strategy by constructing a ternary composite comprising high glass transition temperature fluorene polyester (FPE), polyetherimide (PEI), and high-aspect-ratio γ-Al_2O_3 nanosheets (AO NS). At the molecular scale, the structural compatibility between FPE and PEI enables homogeneous blending, while the incorporation of PEI increases free volume, enhances dipolar mobility, and preserves low dielectric loss. At the nanoscale, AO NS act as ceramic barriers to suppress charge injection, raise interfacial polarization, and stabilize the local electric field. At the device level, this hierarchical design leads to synergistic improvements in dielectric properties, insulation, and energy storage performance. As a result, the optimized composite achieves excellent high-temperature energy-storage capability, characterized by a high energy density of 5.51 J/cm^3 with above 80% efficiency at 150 °C and 550 MV/m. This study paves a practical and scalable path toward high-performance polymer dielectrics for reliable energy storage under extreme thermal and electrical conditions.

© 2026 Published by Elsevier B.V. on behalf of Chinese Chemical Society and Institute of Materia Medica, Chinese Academy of Medical Sciences.

Polymer dielectric capacitors are widely recognized for their rapid charge/discharge rates and exceptional power density, rendering them indispensable in modern electronic and electrical systems [1–5]. Compared to dielectric ceramics, polymer-based counterparts are favored due to their superior breakdown strength, inherent flexibility, and scalability for large-area fabrication [6–8]. However, under combined thermal stimuli and electrical stress, charge injection, excitation, and migration within polymer dielectrics induce an exponential increase in leakage conductance and thereby attenuate the energy-storage capacity [9–12]. These factors inevitably constrain their operational temperature range, failing to meet application requirements in the ever-increasing demand within a harsh environment exceeding 100 °C [4,13]. Thus, developing dielectric polymers that can deliver not only high discharged energy density (U_d) and energy efficiency (η) but also outstanding thermal stability is highly demanded [14,15]. According to electrostatic theory, $U_d = \int_{P_r}^{P_{max}} E dP$ and $\eta = U_d/(U_d + U_{loss})$, where E is the electric field, P_{max} and P_r denote the maximum and remanent polarization, U_{loss} represents energy loss, respectively [6,16,17]. Therefore, it is noteworthy that a large P_{max}, small P_r, high breakdown strength (E_b), along with good insulating properties under high temperature, constitute the foundations for high-temperature and high-performance energy storage.

To address these limitations, various strategies have been developed to optimize polarization behavior and enhance dielectric performance at elevated temperatures. A widely adopted approach involves incorporating heat-resistant polymers with high dielectric constant (ε_r) inorganic oxides or nitrides (*e.g.*, Al_2O_3, HfO_2, SiO_2, BNNS), which possess wide bandgaps and excellent thermal stability [18–23]. These inorganic fillers serve both as charge-blocking barriers and interfacial polarization centers, effectively impeding carrier transport and suppressing leakage currents under high electric fields [24–27]. Another promising method involves hybridizing metal oxide clusters with polymer matrices [28]. The resultant architecture not only leverages the electrical advantages of inor-

* Corresponding authors.
E-mail addresses: tianyuli@ustb.edu.cn (T. Li), xieb@nchu.edu.cn (B. Xie).

https://doi.org/10.1016/j.cclet.2025.111775
1001-8417/© 2026 Published by Elsevier B.V. on behalf of Chinese Chemical Society and Institute of Materia Medica, Chinese Academy of Medical Sciences.

ganic components but also mitigates interfacial incompatibility between organic and inorganic phases, thereby improving dispersion and functional integration [28–31]. Given that dielectric loss and polarization instability are often intensified near the glass transition temperature (T_g), high-T_g polymers, such as polyetherimide (PEI), polycarbonate (PC), and polyimide (PI), are commonly selected as matrix to composite them with other organics through crosslinking [2,32], blending [33–37] or molecular structure tailoring [38–40]. The resulting complex microstructures and interfacial domains can effectively trap thermally activated carriers, enhance thermal resistance, and progressively boost insulating property and energy-storage capability. Despite these advancements, many polymer-based dielectrics still struggle with issues such as filler agglomeration, interfacial mismatch, and reduced mechanical flexibility [7,41]. These limitations may lead to local electric field distortion and early breakdown under coupled thermal-electric stress [35,42]. Moreover, the intrinsic trade-offs among polarization strength, dielectric hysteresis, and breakdown strength, particularly under high-temperature and high electric fields, highlight the urgent need for multiscale design strategies to finely balance these competing parameters and unlock the full potential of polymer-based dielectric materials.

Herein, we present a multiscale chemical configuration-engineered ternary composite comprising high-T_g fluorene polyester (FPE), polyetherimide (PEI), and high-aspect-ratio γ-Al_2O_3 nanosheets (AO NS) to overcome these challenges. At the molecular level, FPE and PEI share comparable backbone architectures and polar functional groups, ensuring intrinsic compatibility and uniform morphology without compromising mechanical integrity. The introduction of PEI selectively expands the free volume and enhances chain-segment mobility, which synergistically augments dipolar orientation and thermal stability. At the nanoscale, AO NS serve as dispersed barriers that drastically increase the tortuosity of the leakage pathways, while their high dielectric constant and interfacial polarization amplify P_{max} and suppress P_r. At the device level, the optimized FPE/PEI-50/AO NS-1.0 composite exhibits a breakdown strength of 662 MV/m and delivers a high discharged energy density of 5.51 J/cm^3 with above 80 % efficiency at 150 °C. Comprehensive experimental characterization, combined with multiscale simulations of free-volume distributions, interfacial field mapping, and electronic energy levels, elucidates the underlying mechanisms governing its exceptionally high-temperature energy-storage capabilities. This work provides a scalable, practical pathway to overcome the performance limitations of dielectric polymers, advancing next-generation high-temperature capacitors for energy systems.

FPE/PEI/AO NS composites were synthesized by a solution-casting method, in which γ-phase alumina nanosheets (γ-AO NS) were prepared through a hydrothermal process (see Supporting information for detailed procedures and X-ray diffraction pattern of as-prepared and high-purity AO NS in Fig. S1 in Supporting information). The molecular structures of FPE and PEI are illustrated in Fig. 1a, demonstrating a high degree of structural similarity, including comparable backbone configurations and functional groups. This molecular-level resemblance indicates strong intrinsic compatibility between the two polymers. To further substantiate this compatibility, molecular dynamics (MD) simulations were conducted. As shown in Fig. 1b, a schematic of the multiscale-engineered ternary composite comprising FPE, PEI, and γ-AO NS is presented, along with a three-dimensional simulated structure reflecting the actual compositional ratios. The simulation confirms a favorable interfacial interaction among the three components, supporting the formation of a structurally coherent hybrid system. Morphological characterization using scanning electron microscopy (SEM) reveals a dense and uniform composite surface, free from visible cracks, voids, or nanoparticle agglomeration. Moreover, energy-dispersive X-ray spectroscopy (EDS) elemental mapping confirms the uniform distribution of nitrogen and aluminum elements within the FPE matrix (Figs. 2a and b). The thermal stability of the composites was further evaluated by thermogravimetric analysis under N_2 atmosphere (Fig. 2c). A closer inspection of the initial decomposition region (Fig. 2d) reveals that the temperatures corresponding to 5 % and 10 % weight loss ($T_{5\%}$ and $T_{10\%}$) increase significantly from 481 °C and 496 °C for pure FPE to 527 °C and 538 °C, respectively, for the FPE/PEI-50/AO NS-1.0 composite. These results collectively affirm that the excellent structural homogeneity, as well as significantly improved thermal stability of the composite, indicate the successful preparation of high-quality dielectric composites following the proposed design strategy.

Dielectric properties and breakdown strength of the composites were subsequently investigated; these are critical parameters governing their energy storage capability. It is well established that a high ε_r value often implies a strong polarization capability and increased potential for dielectric energy storage. As shown in the frequency-dependent dielectric spectra (Fig. 3a), the FPE/PEI-50 binary composite exhibits a higher dielectric constant (*e.g.*, $\varepsilon_r = 3.89$ at 1 kHz) than that of pristine FPE ($\varepsilon_r = 3.12$ at 1 kHz) and PEI ($\varepsilon_r = 3.13$ at 1 kHz). This is because the increased chain spacing and

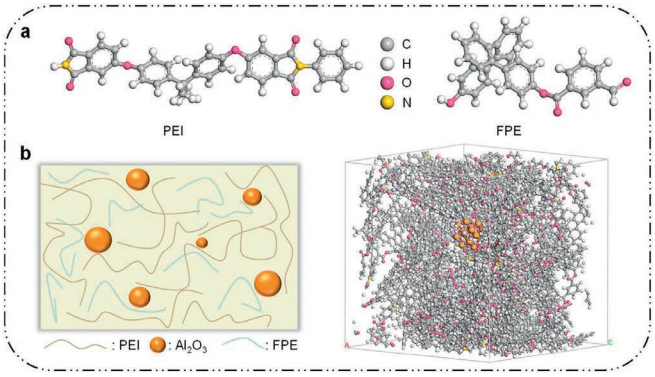


Fig. 1. Schematic illustration of the multiscale chemical configuration design proposed in the FPE/PEI/AO NS composite systems. (a) Molecular structures of PEI and FPE. (b) Schematic diagram (left) and three-dimensional simulation diagram of the ternary blend (right).

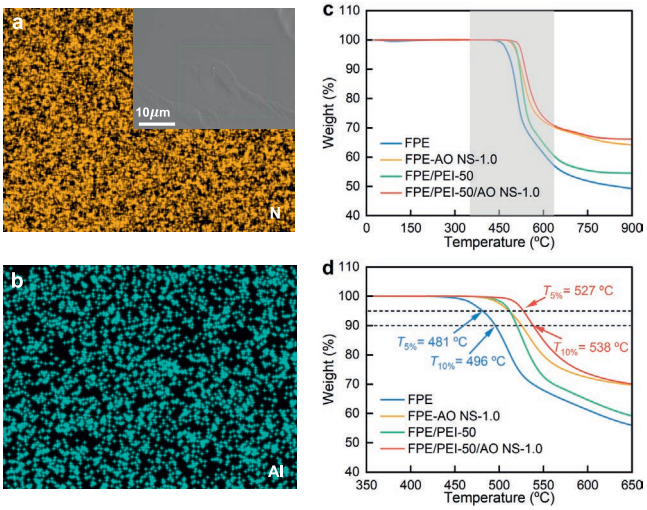


Fig. 2. Microstructure and thermal stability characterizations of the multiscale-engineered ternary composite system. (a, b) SEM image (inset) and EDS maps of the FPE/PEI-50/AO NS-1.0 composite material. (c) TG curve of pure FPE and its composite materials. (d) Local magnified view of the TG curve.

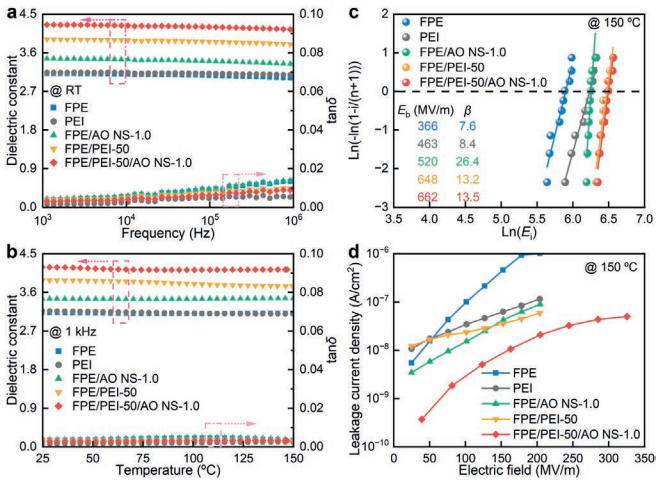


Fig. 3. Measurements of high-temperature dielectric and insulating properties for the multiscale-engineered ternary dielectric composite. Spectra of dielectric constant and dielectric loss of pure polymer and FPE-based composites as a function of (a) frequency and (b) temperature. (c) Two-parameter Weibull distribution and fitting results for breakdown strength and (d) leakage current density as a function of electric field of the polymer-based systems measured at 150 °C.

enlarged free volume induced by blending FPE with PEI, which facilitate dipole reorientation and alignment under applied electric fields, thereby boosting dielectric polarization with minimal energy loss. Upon further incorporation of Al_2O_3 nanosheets, the ε_r value of the FPE/PEI-50/AO NS-1.0 composite increases to 4.25 at 1 kHz, surpassing those of both the FPE/AO NS-1.0 and FPE/PEI-50 binary composites. In addition to the intrinsically high dielectric constant of γ-phase alumina fillers, this further enhancement can be attributed to interfacial polarization effects, namely Maxwell–Wagner–Sillars polarization, which arises from strong interactions between the high-aspect-ratio AO NS and the surrounding polymer chains. These interfacial effects significantly strengthen the composite's overall polarization response, leading to improved dielectric performance. Furthermore, the composites also demonstrate excellent dielectric thermal stability. As shown in Fig. 3b, the ε_r of FPE/PEI-50/AO NS-1.0 decreases by only 2.9 % when the temperature increases from 25 °C to 150 °C. Simultaneously, the dielectric loss remains exceptionally low ($\tan\delta < 0.005$) across this wide temperature range. These results collectively highlight the superior dielectric reliability of the composite under thermal stress and further confirm its strong potential for high-temperature dielectric energy storage applications.

Given that excellent insulating characteristics are essential for achieving high energy-storage performance, we evaluated the high-temperature breakdown strength (E_b) and leakage current density (J) of pure polymer and FPE-based composite materials. The E_b values at 150 °C were determined using a two-parameter Weibull distribution, with the fitting results presented in Fig. 3c. It is noteworthy that the FPE/PEI-50/AO NS-1.0 composite material achieves a maximum breakdown strength of 662 MV/m compared with pure FPE (366 MV/m), PEI (463 MV/m), and FPE-based binary composites (520 and 648 MV/m). The remarkable breakdown performance of the ternary composite is driven by the large band gap and high insulating property of the alumina nanosheet (AO NS) filler, along with the nanostructured morphology impeding carrier immigration and inhibiting the formation of conductive paths under high field. Fig. 3d compares the leakage current density of the different composites, pristine FPE and PEI, wherein the ternary composite exhibits a minimal leakage conductance. Specially, the J value of FPE/PEI-50/AO NS-1.0 decreases from 1.0×10^{-6} A/cm^2 for pure FPE to 2.1×10^{-8} A/cm^2 at 200 MV/m, being significantly lower than other pristine and composite systems, which should be attributed to the optimized dielectric properties and electronic configuration. Therefore, it can be concluded a significantly improved insulating properties for the FPE/PEI/AO NS ternary system, thereby providing a favorable foundation for achieving high-temperature energy storage.

Table 1
P_{max}, P_r, and ΔP values of the polymer systems at 150 °C under their respective maximum electric fields.

Polymer and composite	P_{max} (μC/cm^2)	P_r (μC/cm^2)	ΔP (μC/cm^2)
FPE	1.69	0.42	1.27
PEI	2.14	0.43	1.71
FPE/AO NS-1.0	2.25	0.23	2.02
FPE/PEI-50	2.65	0.52	2.13
FPE/PEI-50/AO NS-1.0	2.81	0.52	2.29

High-temperature polarization behavior of the composites was systematically investigated by measuring their $P-E$ loops. Figs. S2 and S3 (Supporting information) illustrate the comparison of the $P-E$ cycles of the original polymer and its composite material under the conditions of 150 °C and 200 °C. Among them, the FPE/PEI-50/AO NS-1.0 composites endure the highest strength of tolerable electric field, agreeing well with its highest E_b value and lowest leakage conductance, as previously discussed. Benefiting from the easier polarization reorientation/tension within a large free volume and additional contribution of linear polarization from high dielectric constant Al_2O_3 nanosheets, the FPE/PEI-50/AO NS-1.0 composite material possesses large P_{max} and small P_r, as shown in Table 1. Its P_{max} (2.81 μC/cm^2) is the highest among all samples. Compared to pristine FPE ($P_{max} = 1.69$ μC/cm^2), this represents a 66 % improvement, yielding the highest effective polarization ($\Delta P = P_{max} - P_r$) among all tested systems. These results demonstrate that the FPE/PEI-50/AO NS-1.0 composite achieves an optimal balance between high P_{max}, low P_r, and excellent breakdown strength, which is critical for efficient energy-storage performance. Furthermore, the large ΔP value confirms the material's strong potential to achieve high discharged energy density, reinforcing the effectiveness of the ternary design strategy in simultaneously optimizing dielectric, insulating, and polarization characteristics for next-generation polymer-based capacitors.

High-temperature energy-storage capabilities and practical charging-discharging characteristics of the polymer-based composites were subsequently measured (Fig. 4). The electric field-dependent U_d and η were extracted from their respective $P-E$ loops. As expected, FPE/PEI-50/AO NS-1.0 exhibits the highest U_d, reaching up to 6.48 J/cm^3 at a high temperature of 150 °C and an applied electric field of 620 MV/m (Fig. 4a). This value represents a remarkable 241 % improvement over that of pristine FPE, which delivers only 1.9 J/cm^3 at 350 MV/m. Equally noteworthy is the fact that the ternary composite maintains a high U_d of 5.51 J/cm^3 while preserving an efficiency of above 80 % at 150 °C, highlighting its excellent energy retention at elevated temperature. Further measurements at 200 °C (Fig. 4b) show that the FPE/PEI-50/AO NS-1.0 composite still achieves U_d of 3.22 J/cm^3 with an η exceeding 70 % under 440 MV/m, corresponding to a 279 % enhancement compared to the 0.85 J/cm^3 of pure FPE. To investigate the power density of the composite, a fast-discharging experiment was implemented. Fig. 4c and d illustrate the time-dependent charging/discharging energy density and power density under various environmental temperatures (25, 100, and 150 °C), derived from the corresponding current curves. At 150 °C, the FPE/PEI-50/AO NS-1.0 composite demonstrates a rapid discharging time $t_{0.9}$ of 7.24 μs ($t_{0.9}$ is defined as the time to release 90 % of stored energy) and high discharging energy density W_{dis} of 0.77 J/cm^3, leading to an outstanding power density (P_D) of 98.23 MW/L. Collectively, these re-

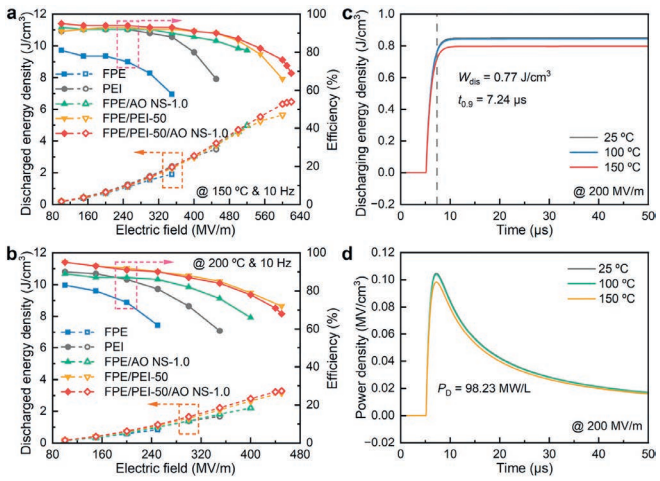


Fig. 4. High-temperature dielectric energy-storage performance of multiscale-engineered polymer composites. Discharged energy density and efficiency of pure FPE and its composite materials measured at (a) 150 °C and (b) 200 °C. (c) Discharging energy density and (d) power density of FPE/PEI-50/AO NS-1.0 composite material measured at various temperatures.

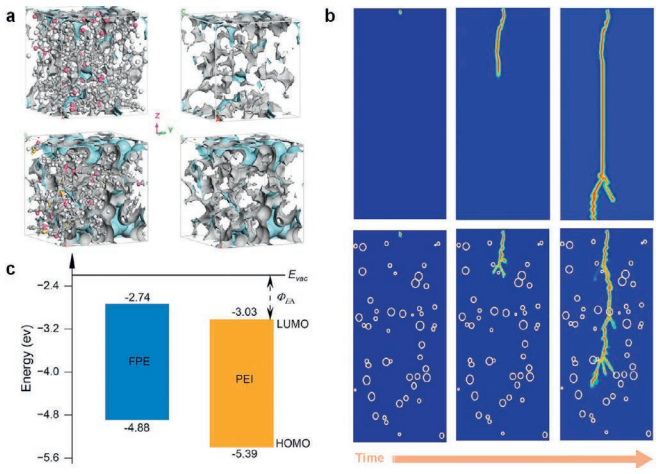


Fig. 5. (a) Free volume simulation of pure FPE and FPE/PEI-50 based on molecular dynamic calculation. (b) Simulation diagram of electric tree breakdown of FPE/PEI-50 (the first row) and FPE/PEI-50/AO NS-1.0 (the second row). (c) Band diagram of FPE and PEI based on density functional theory calculation.

sults unequivocally demonstrate the superior high-temperature dielectric energy storage performance of the FPE/PEI-50/AO NS-1.0 composite. The combination of high energy density, excellent efficiency, and rapid charging-discharging behavior validates the effectiveness of the proposed nanocomposite design strategy for advanced thermal-stable polymer capacitors.

To unravel the underlying physical mechanism governing the optimized electric properties and reinforced energy storage, multiscale theoretical simulations were carried out to corroborate the experimental findings. First, free-volume calculations (Fig. 5a) reveal that blending FPE with PEI enlarges the inter-chain spacing and increases the total free-volume fraction compared with neat FPE. The shaded regions in Fig. 5a quantitatively demonstrate that a higher free volume facilitates dipolar rotation and alignment under an external field, thereby boosting the dielectric constant and polarization while suppressing dielectric loss. The close similarity of ε_r and molecular structure between FPE and PEI ensures good intermolecular compatibility and avoids severe dielectric-mismatch stresses, which further contributes to the high breakdown electric field. Second, continuum-scale electrostatic simulations of the two-dimensional AO NS fillers (Fig. 5b) show that their high-aspect-ratio morphology effectively blocks charge injection from the electrodes, lengthens the branching paths of partial discharges, and stabilizes the local field distribution at elevated temperatures. At the same time, the intrinsic high dielectric constant of AO NS and the Maxwell-Wagner-Sillars interfacial polarization at the filler-polymer boundaries jointly raise the composite ε_r and improve thermal breakdown resistance. Third, our density functional theory calculations of the molecular band structures for FPE and PEI indicate that PEI possesses a deeper LUMO level (Fig. 5c), which corresponds to a larger electron affinity and underlies a higher Schottky barrier at the electrode/dielectric interface. This elevated barrier suppresses electron injection into the bulk under high fields, reducing leakage current density and thus enhancing the dielectric strength. Taken together, these results provide a coherent physical picture: increased free volume and interfacial polarization raise ε_r and P while high-aspect-ratio fillers and Schottky-barrier effects suppress charge injection; and polymer compatibility maintains mechanical integrity, all of which synergistically drive the observed improvements in high-temperature energy-storage performance.

In summary, we present a ternary FPE/PEI/γ-Al_2O_3-nanosheet ternary composite that leverages free-volume engineering and interfacial polarization to achieve a high dielectric constant of 4.13 with very low dielectric loss below 0.005 (at 150 °C, 1 kHz) and high breakdown strength of 662 MV/m, delivering a superior high-temperature energy-storage performance of energy density up to 5.51 J/cm^3 at $\eta > 80\%$ and 150 °C. By combining experimental findings with multiscale simulations, we identify that PEI's deeper lowest unoccupied molecular orbital suppresses leakage currents, while high-aspect-ratio alumina nanosheets stabilize local electric fields and impede the formation of breakdown paths. The proposed design paradigm in this study provides a versatile strategy for next-generation polymer capacitors operating under extreme thermal and electrical conditions.

Declaration of competing interest

The authors declare that they have no known competing financial interests or personal relationships that could have appeared to influence the work reported in this paper.

CRediT authorship contribution statement

Yuyan Du: Writing – original draft, Visualization, Methodology, Investigation, Formal analysis, Data curation, Conceptualization. **Jinxia Cai:** Methodology, Investigation, Formal analysis, Data curation. **Tianyu Li:** Writing – review & editing, Writing – original draft, Supervision, Resources, Funding acquisition, Conceptualization. **Yandong Hu:** Investigation, Formal analysis, Data curation. **Haibo Zhang:** Supervision, Resources, Project administration. **Bing Xie:** Writing – original draft, Supervision, Resources, Methodology, Funding acquisition, Conceptualization.

Acknowledgments

This work is supported by the National Natural Science Foundation of China (No. 52162018), Science Fund for Distinguished Young Scholars of Jiangxi Province (No. 20224ACB214007), the Aeronautical Science Foundation of China (No. 2020Z056056001), China Postdoctoral Science Foundation (No. 2024M760202), and China National Postdoctoral Program for Innovative Talents (No. BX20240035).

Supplementary materials

Supplementary material associated with this article can be found, in the online version, at doi:10.1016/j.cclet.2025.111775.

References

[1] D. Yue, J.H. Yin, W.C. Zhang, et al., Adv. Funct. Mater. 33 (2023) 2300658.
[2] M. Yang, M. Guo, E. Xu, et al., Nat. Nanotechnol. 19 (2024) 588–603.
[3] R. Wang, Y. Zhu, S. Huang, et al., Nat. Mater. 24 (2025) 1074–1081.
[4] X.J. Liu, M.S. Zheng, G. Chen, et al., Energy Environ. Sci. 15 (2022) 56–81.
[5] L. Zhao, F. Zhang, H. Hu, Microstructures 5 (2025) 2025085.
[6] L. Wen, J. Chen, J. Liang, et al., Natl. Sci. Rev. 4 (2017) 23–25.
[7] J. Chen, Z. Pei, B. Chai, et al., Adv. Mater. 36 (2023) 2308670.
[8] H. Luo, F. Wang, R. Guo, et al., Adv. Sci. 9 (2022) e2202438.
[9] C. Yuan, Y. Zhou, Y. Zhu, et al., Nat. Commun. 11 (2020) 3919.
[10] J.S. Ho, S.G. Greenbaum, ACS Appl. Mater. Interfaces 10 (2018) 29189–29218.
[11] D. Tan, L. Zhang, Q. Chen, et al., J. Electron. Mater. 43 (2014) 4569–4575.
[12] Q. Li, F.Z. Yao, Y. Liu, et al., Annu. Rev. Mater. Res. 48 (2018) 219–243.
[13] X. Li, P. Hu, J. Jiang, et al., Adv. Mater. 37 (2025) 2411507.
[14] Q.K. Feng, S.L. Zhong, J.Y. Pei, et al., Chem. Rev. 122 (2021) 3820–3878.
[15] J.W. Zha, M. Xiao, B. Wan, et al., Prog. Mater. Sci. 140 (2023) 101208.
[16] B. Fan, M. Zhou, C. Zhang, et al., Prog. Polym. Sci. 97 (2019) 101143.
[17] G.Q. Ma, T.B. Yang, D.L. Li, et al., ACS Appl. Mater. Interfaces 15 (2023) 23701–23710.
[18] H. Li, T. Yang, Y. Zhou, et al., Adv. Funct. Mater. 31 (2020) 2006739.
[19] D. Ai, H. Li, Y. Zhou, et al., Adv. Energy Mater. 10 (2020) 1903881.
[20] B. Sun, P. Hu, X. Ji, et al., Small 18 (2022) 2202421.
[21] P. Wang, Y. Guo, D. Zhou, et al., Adv. Funct. Mater. 32 (2022) 2204155.
[22] L. Li, J. Dong, R. Hu, et al., Chem. Eng. J. 435 (2022) 135059.
[23] S. Zhang, B. Xie, J. Cai, et al., Nanoscale 17 (2025) 16447–16456.
[24] S. Cheng, Y. Zhou, Y. Li, et al., Energy Storage Mater. 42 (2021) 445–453.
[25] P. Yin, L. Lei, Q. Tang, et al., Energy Storage Mater. 77 (2025) 104213.
[26] G. Liu, L. Zhu, Z. Chang, et al., Adv. Funct. Mater. 35 (2025) 2425001.
[27] Z. Ren, L. Lei, L. Zhu, et al., Adv. Funct. Mater. 35 (2024) 2417156.
[28] Z. Pan, Y. Cheng, Z. Li, et al., Energy Environ. Sci. 18 (2025) 4405–4415.
[29] S. Zhao, W. Peng, L. Zhou, et al., Nat. Commun. 16 (2025) 769.
[30] M. Fiaz, J. Lin, S. He, Mater. Today 47 (2021) S121–S124.
[31] H. Li, Z. Xie, C. Yang, et al., Nano Energy 113 (2023) 108544.
[32] H. Li, M.R. Gadinski, Y. Huang, et al., Energy Environ. Sci. 13 (2020) 1279–1286.
[33] J. Chen, Y. Zhou, X. Huang, et al., Nature 615 (2023) 62–66.
[34] M. Yang, W. Ren, M. Guo, et al., Small 18 (2022) 2205247.
[35] L. Zhou, S. Zhao, P. Xie, et al., Appl. Phys. Rev. 10 (2023) 031310.
[36] Y. Shang, Y. Feng, Z. Meng, et al., Mater. Horiz. 11 (2024) 1528–1538.
[37] J. Wang, H. Guo, S. Zeng, et al., Chem. Eng. J. 492 (2024) 152237.
[38] Z. Zhang, J. Zheng, K. Premasiri, et al., Mater. Horiz. 7 (2020) 592–597.
[39] C. Wu, A.A. Deshmukh, L. Chen, et al., Matter 5 (2022) 2615–2623.
[40] Q. Zhang, Q. Xie, T. Wang, et al., Nat. Commun. 15 (2024) 9351.
[41] X. Chen, H. Qin, Y. Liu, et al., Appl. Phys. Lett. 122 (2023) 212901.
[42] Z. Zhao, S. Zhang, M. Li, et al., J. Appl. Phys. 135 (2024) 194103.